ACADEMIC PRESS

Available online at www.sciencedirect.com

SCIENCE DIRECT®

Cryobiology 46 (2003) 254–263

CRYOBIOLOGY

www.elsevier.com/locate/ycryo

Thermal expansion measurements of cryoprotective agents. Part I: A new experimental apparatus☆

Yoed Rabin* and Ernest Bell

Department of Mechanical Engineering, Carnegie Mellon University, 5000 Forbes Avenue, Pittsburgh, PA 15213, USA

Received 14 January 2003; accepted 15 April 2003

Abstract

As part of an ongoing effort to characterize the mechanical behavior of biological tissues in the cryogenic temperature range, the current study focuses on the thermal expansion measurements of cryoprotective agents. This study focuses on the upper part of the cryogenic temperature range, where the cryoprotectant behaves like low viscous liquid at all practical cooling rates. For the purpose of this study, a new apparatus for thermal expansion measurements has been designed and constructed. Part I of this study (the current report) includes: a description of the new experimental apparatus, the techniques of operation, calibration, system validation, and a detailed uncertainty analysis. Part II of this study (the report following) includes thermal expansion measurements of the cryoprotectant mixtures DP6 and VS55, and comparison with data from the literature on DMSO solutions.

Keywords: Cryopreservation; Cryoprotectant; Solid mechanics; Thermal expansion

The volume change associated with change in temperature of the material is known as 'thermal expansion.' The ratio of the thermal expansion to the initial volume is known as 'volumetric thermal strain.' The term 'linear thermal strain' is defined as one third of the volumetric thermal strain. The term 'linear thermal expansion coefficient' represents a physical property indicating the rate at which the linear thermal strain changes with temperature. A positive value of the linear thermal expansion coefficient indicates an increase in volume with the increase in temperature (volume expansion), while a negative value indicates a decrease in volume with the increase in temperature (volume contraction). In the context of this report, the term 'thermal expansion' is used as a generic term indicating the physical process, irrespective of the sign of the linear thermal expansion coefficient. Unless otherwise specified, the terms 'linear thermal strain' and 'thermal strain' have the same meaning in this report. Likewise, the terms 'linear thermal expansion coefficient' and 'thermal expansion coefficient' have the same meaning.

If the material is constrained, thermal strain leads to the development of mechanical stress, either in fluids or in solids. In stationary fluids, this

☆ This work was funded by institutional sources.
* Corresponding author. Fax: 1-412-268-3348.
E-mail address: rabin@cmu.edu (Y. Rabin).

0011-2240/03/$ - see front matter
doi:10.1016/S0011-2240(03)00042-7

stress is known as 'hydrostatic pressure.' In solids, this stress is conveniently presented as the combination of hydrostatic pressure and shear stress [1,11,12,16,17]. Either way, thermal strain can lead to high levels of stress, resulting in structural damage due to fracture formation and/or plastic deformations [12,13]. In the context of cryobiology, even a single macro fracture, or large enough region to plastically deform, can prevent recovery of the biological tissue from cryogenic preservation. Volumetric strain in liquids and solids is typically measured in a magnitude range $0–10^{-2}$, where a magnitude of 10^{-2} in a constrained material is typically associated with structural damage in solids [12,13].

One driving mechanism of thermal expansion is the tendency to increase the typical distance between molecules with an increase in temperature. Another driving mechanism of thermal expansion is molecular rearrangement during the process of crystallization. Similar expansion may take place due to molecular rearrangement associated with solid–solid phase change. Although thermal expansion associated with crystallization may be associated with very small temperature changes, the outcome can be quite dramatic. For example, pure water crystallization is associated with 9% increase in volumetric thermal strain. If liquid water is encapsulated in an ice enclosure, a thermal strain of such magnitude can easily lead to structural damage in the solid phase, and to dramatic hydrostatic pressures in the liquid phase [14,15,17].

Mechanical stress is only one of several mechanisms of cryoinjury. A far more extensively studied mechanism of cryoinjury is ice crystal formation, either in the extracellular or the intracellular space, which triggers a sequence of destructive events at the cellular level [6,10]. Cellular level damage can lead to macro level effects when it affects the vascular system, the neural system, or when the overall volume of damaged cells is statistically significant.

In order to avoid the damaging effect of crystal formation on biological cells, an alternative approach to cryopreservation has been suggested, known as 'vitrification' (vitreous in Latin means glass) [3–5,9]. Vitrification is a highly unstable process in which solidification is achieved by rapid elevation of viscosity, until the level is high enough that the material can be considered solid for all practical purposes. In order to suppress crystallization and promote vitrification, highly viscous solutions, known as 'cryoprotectants,' are introduced into the biological specimen. However, the identification of a vitreous material as a solid is a matter of time-scale only. The vitreous material can be considered liquid in slow thermo-mechanical loading processes, while the vitreous material can be considered solid in rapid processes. The demarcation between slow and rapid is proportional to the level of viscosity of the material, which in turn, is dependent upon the temperature. In general, viscosity increases exponentially with the decrease in temperature. In the solid mechanics' sense, whether the vitreous material is likely to develop structural damage or to comply with the thermal strain, is dependent upon the ratio of viscosity to the time-scale of the thermal loading.

As a part of an ongoing effort to characterize the mechanical behavior of biological tissues in cryogenic temperature range [2,11–17], the current study focuses on thermal expansion measurements of cryoprotectants. The measured parameter is the volumetric thermal strain and the analyzed thermophysical property is the thermal expansion coefficient. The current study focuses on the upper part of the cryogenic temperature range, where the cryoprotectant can be considered low viscosity liquid at all practical cooling rates, whether during vitrification or during classical cryopreservation. In the solid mechanics sense, liquid can be defined as a material which continues to deform under the application of a constant load; low viscosity indicates that the deformation rate is relatively high for low loads. The current study also addresses the effect of volume change associated with crystallization. For the purpose of this study, a new apparatus for thermal expansion measurements has been designed and constructed. The new device is based on a new concept in which pressure is the measured physical phenomenon and the relationship between pressure and thermal expansion is correlated. The current report includes two parts: Part I includes a description of the new experimental apparatus, techniques of operation, calibration, system validation, and

a detailed uncertainty analysis. Part II includes thermal expansion measurements of the cryoprotectant mixtures DP6 and VS55, and comparison with available data from the literature on DMSO solutions.

Experimental apparatus

Figure 1 presents a schematic illustration of the experimental apparatus. The cooling chamber is made from two copper stub-out tubes. A stub-out tube is a cylindrical tube having one closed end in a shape of a hemisphere, which is used to prevent the water hummer effect in domestic water tubing. The nominal diameter of the stub-out tube is 1/2 in., and the wall thickness is 1.25 mm. The stub-out tubes are connected with standard 1/2 in. male and female copper adapters. The stub-out tubes were shortened so that the volume enclosed in the assembly is 11.1 ± 0.05 ml (the overall length of the cooling chamber is about 90 mm). Two holes were drilled at the upper part of the cooling chamber to accommodate a filling valve and a pressure tube (pressure tube B in Fig. 1), where sealing was achieved by soldering. The filling valve is made from the following: (i) a copper tube having an external diameter of 1.6 mm, internal diameter of 0.8 mm, and a length of 30 mm and (ii) a 1/16 in. fitting plug of Swagelock. Pressure tube B is made of copper, having an external diameter of 1.6 mm, internal diameter of 0.8 mm, and a length of 150 mm. Using 1/16 in. Swagelock connector, two pressure tubes are connected in series to pressure tube B: (i) a flexible Tygon tube, having internal diameter of 0.51 mm, an external

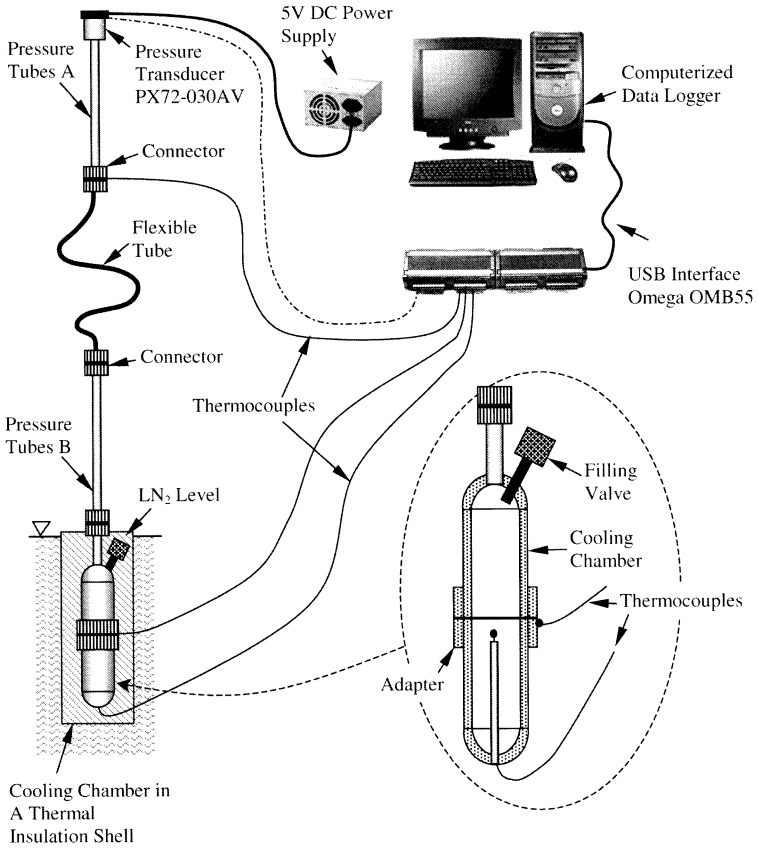

Figure 1. Schematic illustration of the experimental apparatus.

diameter of 1.52 mm, and a length of 500 mm and (ii) a copper tube (pressure tube A in Fig. 1), having an internal diameter of 0.8 mm, an external diameter of 1.6 mm, and a length of 300 mm. The cooling chamber, including the filling valve and the first 50 mm of pressure tube B, are placed in a Styrofoam thermal insulation shell, having an average thickness of 15 mm. The purpose of the thermal insulation shell is to passively control the cooling rate at the cooling chamber, as described below. Furthermore, the relatively thick wall of the thermal insulation shell and the high thermal conductivity of the copper wall of the cooling chamber, are expected to create a close-to-uniform temperature distribution along the cooling chamber wall.

A miniature pressure transducer (Omega, PX72-030AV) is connected at the other end of pressure tube A. This pressure transducer measures the absolute pressure in the range 0–30 psi (14.7 psi equals one standard atmospheric pressure). The pressure transducer is excited by a 5 V DC digital power supplier (Bestric, BPS-2004CS-4), which is similar to the power supplier in a regular desktop computer. The specifications of the pressure transducer at 5 V DC excitation are: sensitivity of 7 mV/psi, linearity of 0.5% FS, repeatability of 0.3% FS, and internal temperature compensation in the temperature working range −15–85 °C. The experimental system has been calibrated with respect to the actual sensitivity of the pressure transducer, as described in detail below.

A desktop computer is used as a digital data logger, collecting experimental data through a USB interface device (Omega, OMB-DAQ55). Collected experimental data include: pressure transducer output, excitation voltage, temperature of the connector of pressure tube A, wall temperature of the cooling chamber, temperature at the center of the cooling chamber, and room temperature (not shown in Fig. 1). All temperature sensors are special T type thermocouples, having a typical uncertainty range of ±0.5 °C.

System preparations

The initial temperature of the measured sample, and all pressure tubes, is room temperature, in the range 20–22 °C. While pressure tube A is open to the surroundings, room atmospheric pressure is measured for reference.

Next, the flexible tube is connected to pressure tube B at one end, while the other end of the flexible tube remains open and is held at a higher level than the filling valve of the cooling chamber. Using a syringe, a solution sample (a cryoprotectant) is injected into the cooling chamber through the filling valve. When the cooling chamber, pressure tube B, and the flexible tube, are completely filled with the solution sample (the flexible tube is transparent), the filling valve is locked, and pressure tube A is connected. Pressure tube A contains air only, and is held at a higher level than the flexible tube and pressure tube B. At this stage, the pressure transducer at one end, and the filling valve at the other end, create a pressure-bearing enclosure for the solution sample. From this point on, any volume change of the chamber, tubes, and solution sample, will generate pressure. Since the compressibility of air is at least three orders of magnitude higher than that of all other components of the system, the combined thermal expansion of all other components of the system is equal to the air volume change. Finally, the cooling chamber is placed in a thermal insulation shell, and the system is ready for experimentation.

Technique of operation

Cooling phase

The thermal insulation shell is immersed in liquid nitrogen to the top of the thermal insulation shell. The flexible tube allows for immersion of the cooling chamber while keeping the pressure transducer and its wiring stationary. As a result of liquid nitrogen boiling on the outer surface of the thermal insulation shell, the temperature of the cooling chamber decreases. Due to the thick thermal insulation, the cooling rate of the cooling chamber is kept at an average rate of 0.85 °C/min in all experiments reported in part II of this study. The low cooling rate leads to a close-to-uniform temperature distribution in the measured sample, typically in the range of up to 3 °C (demonstrated in the second part of this report). In the absence of the thermal insulation, an average cooling rate of

96 °C/min was measured. However, due to the bulky dimensions of the cooling chamber, a significant temperature difference is observed at such a high cooling rate.

Temperature measurements at the center of the cooling chamber and the outer surface of the cooling chamber wall are continually measured; these measurements are later used to estimate the average sample temperature and the maximum temperature difference in the sample at any given point in the process. Pressure measurements are taken continually in order to correlate measured sample volume changes with pressure changes. Calibration of volume to pressure changes is addressed in detail below.

Although the pressure transducer output is electronically compensated for a relatively wide working temperature range −15–85 °C, and in order to decrease the level of uncertainty in pressure measurements, the pressure transducer is placed at a far distance from the cooling chamber, where the temperature remains constant throughout the experiment (i.e., room temperature). For this purpose, a temperature sensor is connected to the 1/16-in. Swagelock connector of the pressure tube A; this thermocouple indicates whether the tube temperature deviates from room temperature. The cooling phase continues until the pressure in tube A reaches steady state.

Rewarming phase

At the beginning of the rewarming stage, the cooling chamber, including its thermal insulation, are pulled out from the liquid nitrogen, and placed in still air at normal room temperature. Heat transfer by free convection prevails from the outer surface of the thermal insulation to the surroundings, which resulted in an average heating rate of 0.7 °C/min in all experiments reported in part II of this study. Pressure and temperature measurements are taken by the same method as in the cooling phase.

Data analysis

The compressibility of liquids is at least three orders of magnitude smaller than that of gasses [14]. The underlying assumption for data analysis in this study is that the cryoprotectant solution can be considered incompressible with respect to the compressibility of air. Hence, any thermal expansion of the solution sample, contained in the cooling chamber, leads to an identical expansion in magnitude—but opposite in sign—of the air volume contained in pressure tube A. Since air is a compressible fluid, the expansion of air, and hence the thermal expansion of the sample, can be correlated with air pressure measurements in the pressure tube A. It follows that air pressure is the measured phenomenon in the experimental apparatus, and the analysis presented below describes the correlation between the air pressure and the thermal expansion of the measured sample. Another underlying assumption in data analysis is that the fluid mechanics problem in the experimental apparatus is primarily hydrostatic, and that any friction forces associated with fluid flow in the various tubes can be neglected.

The correlation between air pressure and air volume changes was measured experimentally as follows. A 1-ml syringe was connected to pressure tube A, using an 1/16 in. Swagelock connector placed on an hypodermic needle. The syringe piston was pulled out manually, starting from zero displacement, while pressure readings versus air displacement were recorded (the smallest division of the syringe is 0.01 ml). During this process, both pressure tube A and the pressure transducer were kept at normal room temperature range 20–22 °C. Figure 2 presents experimental results of pressure versus displacement based on 14 calibration experiments. The best fit polynomial approximation of results (shown in Fig. 2) is referred to as the 'calibration curve' herein.

Data analysis of a typical experiment is performed as follows. The cooling chamber temperature and the corresponding air pressure are tabulated in 2 s intervals. For each point in time, t_i, the pressure difference is calculated:

$$\Delta P_i = P_i - P_0, \tag{1}$$

where P_0 is the initial pressure (about 14.7 psi). The representative sample temperature at time t_i is the numerical average of the temperature values measured at the center of the cooling chamber and at the cooling chamber wall (Fig. 1).

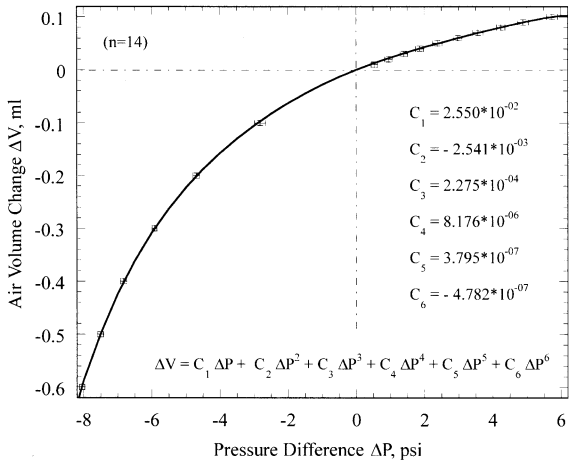

Figure 2. Correlation between air volume changes in pressure tube A, ΔV, and pressure transducer reading, ΔP.

Next, the pressure difference ΔP_i is converted into volume change ΔV_i using the calibration curve. The value of ΔV_i includes both the thermal expansion of the sample and the thermal expansion of the cooling chamber. The thermal strain of the specimen is calculated by:

$$\varepsilon_i = \frac{1}{3}\frac{(\Delta V_i + \Delta V_{cu})}{V_0}, \tag{2}$$

where ΔV_{cu} is the volume expansion of the copper cooling chamber from the initial temperature T_0 to temperature T_i, and where V_0 is the initial volume of the cooling chamber. The change in cooling chamber volume is calculated by:

$$\Delta V_{cu} = 3V_0 \int_{T_0}^{T_i} \beta_{cu}\, dT, \tag{3}$$

where β_{cu} is the thermal expansion coefficient of copper [14].

Next, the thermal strain data, Eq. (2), is represented by a polynomial approximation, based on a least-square approximation technique. Finally, the thermal expansion coefficient of the specimen is calculated by:

$$\beta = \frac{\partial \hat{\varepsilon}}{\partial T}, \tag{4}$$

where $\hat{\varepsilon}$ is the polynomial approximation of the thermal strain based on all data points ε_i.

While the thermal expansion coefficient β is an intrinsic property, which is independent on the technique of measurement, the thermal strain ε is an integral property (the integral of the thermal expansion coefficient with respect to temperature), which is dependent on initial conditions. A variation of initial temperature in the range of ±2 °C, and a variation of initial pressure in the range of ±0.1 psi, are typical between consecutive experiments in the experimental apparatus. In order to increase the statistical significance of the approximation of $\hat{\varepsilon}$, the data analysis is based on n separate experiments in similar conditions. Since each experiment starts with slightly different initial conditions, the experimentally obtained values for ε_i from a specific experiment j ($j = 1, \ldots, n$) may need to be shifted in ε direction on the ε–T plane, so that sets of results from different experiments closely overlap. For this purpose, a results set of one of the experiments ($j = 1$) is arbitrarily selected as a reference, and a polynomial approximation $\hat{\varepsilon}_1$ for this selection is calculated. Next, a results set of a second experiment is selected ($j = 2$), and all data points are shifted by a constant value $\Delta\varepsilon_j$ in order to minimize F_j, which is defined as:

$$F_j = \sum_i [\hat{\varepsilon}_1 - (\varepsilon_i - \Delta\varepsilon_j)]^2. \tag{5}$$

This process is repeated for the entire set of experiments ($j = 2, \ldots, n$), where each experiment requires a different value of $\Delta\varepsilon_j$. Finally, a polynomial approximation $\hat{\varepsilon}$ is calculated based on experimental data from all n experiments combined.

System validation

In order to validate the experimental apparatus, measurement technique, and data analysis, a set of eight experiments has been performed on pure water in the temperature range 20–75 °C. The thermal expansion coefficient of pure water was compiled from data in the literature on water density [8] as follows: (i) a set of water density values and corresponding temperatures in the range 20–75 °C was listed; (ii) the specific volume was calculated as the inverse of the density for the

listed values, where the specific volume at 20 °C was selected as reference; (iii) the difference between the specific volume at each temperature data point, and the reference value was calculated; (iv) the linear thermal strain was calculated as one third of the ratio of the specific volume difference to the specific volume value at the reference point; (v) using a least-square approximation technique, a third-order polynomial approximation was obtained for the thermal strain; (vi) the thermal expansion coefficient was calculated as the first derivative of thermal strain with respect to temperature.

Figure 3 presents experimental results for the thermal strain of water ($n = 8$). The initial condition of each experiment represents zero thermal strain, where the thermal strain is negative in cooling experiments, and positive in heating experiments. Following the procedure described in the data analysis section of this report (Eq. (5)), the thermal strain data was shifted, and the results are shown in Fig. 4.

Figure 4 presents a comparison of experimental measurements and literature data for thermal expansion coefficient (left y scale), and for thermal stain (right y scale). For thermal strain, symbols represent experimental measurements, a solid line represents a third-order polynomial approximation of experimental measurements, and a dashed line represents a third-order polynomial approximation of the literature data. The thermal expansion coefficients of both polynomial approximations are presented in Fig. 4 as the derivative of the thermal strain. From Fig. 4 it can be seen that the experimental system and the data analysis procedure produce highly repeatable results. The thermal strain difference between experimental and literature data is less than 2% of full scale, within the temperature range 20–75 °C. The difference in thermal expansion coefficient between the experimental results and literature data is in the range 17% at 20 °C to 1.5% at 75 °C. Note that the integral quantity of thermal strain is actually used in solid mechanics analysis, while the actual value of the thermal expansion coefficient is not used. It follows that the propagation of uncertainty in measurements in solid mechanics analysis is proportional to the uncertainty in thermal strain, and not to the thermal expansion coefficient [18].

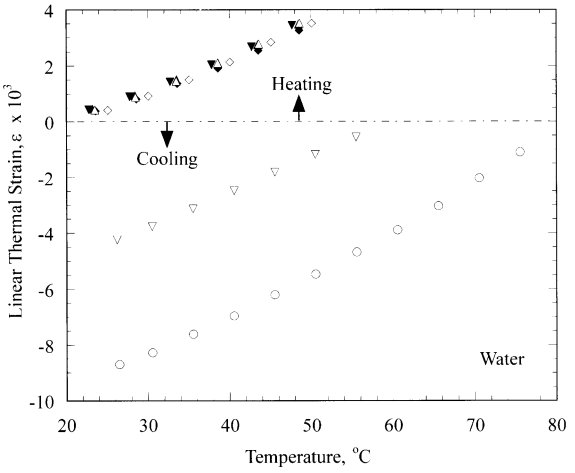

Figure 3. Validation of the experimental apparatus, measurement technique, and data analysis: measurements of linear thermal strain of pure water. The linear thermal strain is an integral property, where positive signs refer to water heating (increase in volume) and negative signs refer to cooling (decrease in volume).

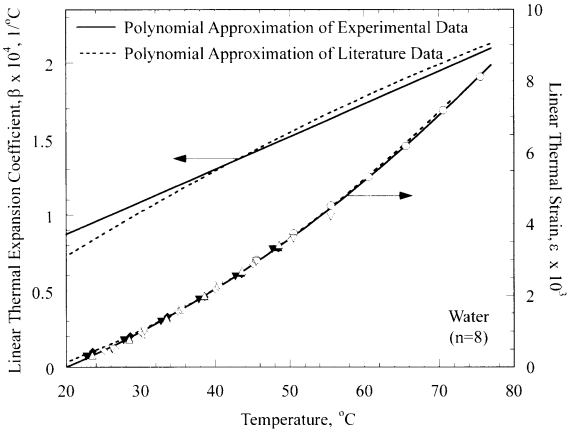

Figure 4. Validation of the experimental apparatus, measurement technique, and data analysis: comparison with water data from the literature [8].

Uncertainty in measurements

Uncertainty in thermal strain calculations results from two independent sources: volume

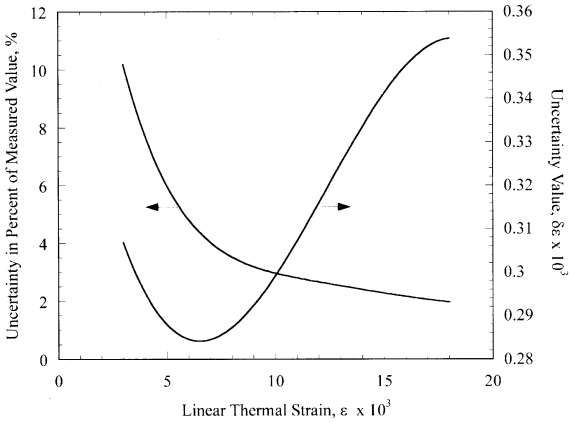

Figure 5. Estimated uncertainty in linear thermal strain calculations as a results of uncertainties in: temperature measurements, pressure measurements, A/D conversion, calibration error, and initial volume measurement (see appendix for detail).

measurements and temperature measurements. While uncertainty in volume measurements directly affects the value of the calculated thermal strain, uncertainty in temperature measurements affects the estimated location of the thermal strain on the temperature scale. As can be seen from Eq. (4), uncertainty in thermal expansion coefficient calculations depends on both independent sources of uncertainty: strain and temperature. The overall uncertainty in strain measurements is estimated in the range 0.28×10^{-3} to 0.36×10^{-3}, as presented in Fig. 5. The overall uncertainty in temperature sensing is estimated as $\pm 0.8\,^{\circ}\mathrm{C}$. Typical uncertainty in the calculated thermal expansion coefficient value is expected to be less than 1% of the calculated value. Detailed uncertainty analysis is included in the appendix of this report.

Summary

As part of an ongoing effort to characterize the mechanical behavior of biological tissues in the cryogenic temperature range, the current study focuses on thermal expansion measurements of cryoprotectants. The measured parameter is the volumetric thermal strain and the analyzed thermophysical property is the thermal expansion coefficient. The current study focuses on the upper part of the cryogenic temperature range, where the cryoprotectant behaves as liquid at all practical cooling rates. For the purpose of this study, a new apparatus, for thermal expansion measurements of liquids in cryogenic temperatures, has been designed and constructed. The apparatus is based on a new concept in which pressure is the measured physical phenomenon for thermal expansion calculations. The current part of the report (part I) includes: a description of the new experimental apparatus, the techniques of operation, calibration, system validation, and a detailed uncertainty analysis.

Comparison of experimental results with data compiled from the literature indicates that the proposed apparatus and technique are adequate for the purpose of thermal expansion measurements. Validation testing on pure water showed that the thermal strain difference between experimental results and data available from the literature is less than 2% of full scale within the temperature range 20–75 °C. The difference in thermal expansion coefficient between experimental results and data available from the literature is in the range of 17% at 20 °C to 1.5% at 75 °C. Note that the integral quantity of thermal strain is used in solid mechanics analysis, and not the actual value of the thermal expansion coefficient. It follows that the propagation of uncertainty in measurements into solid mechanics' analysis is proportional to the uncertainty in thermal strain measurements' and not to the value of the thermal expansion coefficient.

Appendix A. Uncertainty analysis

Uncertainty in strain calculation

It can be seen from Eq. (2) that the strain is a function of the volume change of the sample, ΔV_i, the volume change of the copper cooling chamber, ΔV_{cu}, and the initial volume, V_0. Following a standard engineering analysis of uncertainty [8,18], the uncertainty in the calculated strain can be estimated by:

$$\delta\varepsilon_i = \sqrt{\left[\frac{\partial\varepsilon_i}{\partial(\Delta V_i)}\delta V_i\right]^2 + \left[\frac{\partial\varepsilon_i}{\partial(\Delta V_{cu})}\delta V_{cu}\right]^2 + \left[\frac{\partial\varepsilon_i}{\partial(V_0)}\delta V_0\right]^2}, \tag{A.1}$$

where δV_i is the uncertainty in measurement of ΔV_i, δV_{cu} is the uncertainty in measurement of ΔV_{cu}, and δV_0 is the uncertainty in measurement of V_0.

The partial derivatives in Eq. (A.1) can be directly calculated from Eq. (2):

$$\delta\varepsilon_i = \sqrt{\left[\frac{1}{3V_0}\delta V_i\right]^2 + \left[-\frac{1}{3V_0}\delta V_{cu}\right]^2 + \left[\frac{1}{3}\left(\frac{\Delta V_i - \Delta V_{cu}}{V_0^2}\right)\delta V_0\right]^2}. \tag{A.2}$$

Since the uncertainty in measurement of ΔV_i is expected to far exceed the uncertainty in measurement of ΔV_{cu} (copper data is available in the literature at high certainty), and with reference to the terms within the square root of Eq. (A.2), the upper limit for the sum of the first two terms from the left is twice the value of the first term. The definition of ε_i can further be introduced into the third term from left in the square root, and Eq. (A.2) can be simplified to:

$$\delta\varepsilon_i \leqslant \sqrt{2\left[\frac{1}{3V_0}\delta V_i\right]^2 + \left[\frac{\varepsilon_i}{V_0}\delta V_0\right]^2}. \tag{A.3}$$

As described in Experimental apparatus, $V_0 + \delta V_0 = 11.1 \pm 0.05$ ml. The term δV_i consists of six major sources of uncertainty: (i) repeatability of the pressure transducer, (ii) gain error of the power supply of the pressure transducer, (iii) USB based A/D conversion, (iv) calibration error due to the pressure transducer uncertainty (see x error bars in Fig. 2), (v) uncertainty in syringe piston displacement during calibration (see y error bars in Fig. 2), and (vi) expansion of the solution sample in pressure tube B (the only pressure tube with non-uniform temperature distribution). The uncertainty magnitude of the above sources is proportional to the measured volume, ΔV_i. Figure 5 presents an estimation for $\delta\varepsilon_i$ based on Eq. (A.3), and all sources of uncertainty listed above. Figure 5 also presents the relative error as a function of the strain ε_i. It can be seen that the relative error decreases as the experiment progresses.

The uncertainty value shown in Fig. 5 is for an isolated measurement at a specific point i. However, the process of data analysis, presented above, increases the level of certainty by repeating each experiment several times (decreasing the uncertainty associated with repeatability), and by curve-fitting the results (decreasing the uncertainty associated with random errors at a much higher frequency than the duration of the experiment). Furthermore, strain difference, and not the absolute value of strain, is required for the analysis in solid mechanics. Hence, the effect of systematic error in the experimental system will disappear in solid mechanics' analysis. From the above consideration and the uncertainty definition in Eq. (A.3), the uncertainty estimation in Fig. 5 can be treated as very conservative estimation of uncertainty. Comparison of data from the literature and experimental results in Fig. 4 supports this conclusion.

Uncertainty in temperature calculation

Uncertainty in temperature measurements, δT_i, consists of three major sources: (i) cold junction compensation (± 0.5 °C), (ii) thermocouple readings at 3 Hz (± 0.4 °C), and (iii) quality of the thermocouple material (± 0.5 °C). Using the rule of the square root of the sum of the square errors, the overall uncertainty in temperature sensing is estimated as ± 0.8 °C.

Uncertainty in thermal expansion coefficient calculation

The definition of the thermal expansion coefficient is given in Eq. (4), which is a function of two independently measured properties: strain and temperature. Uncertainty in thermal expansion coefficient calculations is a function of uncertainties in strain and temperature as follows [7]:

$$\delta\beta = \sqrt{\left(\frac{\partial\beta}{\partial T}\delta T\right)^2 + \left(\frac{\partial\beta}{\partial\varepsilon}\delta\varepsilon\right)^2} = \sqrt{\left(\frac{\partial\beta}{\partial T}\delta T\right)^2 + \left(\frac{1}{\beta}\frac{\partial\beta}{\partial T}\delta\varepsilon\right)^2}. \tag{A.4}$$

The upper limit for $\delta\varepsilon$, and the typical value of δT, have been discussed in the previous two sections of this report. The estimation of $\delta\beta$ is dependent on

the temperature dependency of the thermal expansion coefficient, which is unique to the investigated sample. As discussed in the second part of this report, a typical value of β is $2 \times 10^{-4}\,^{\circ}\mathrm{C}^{-1}$, and a typical value of $\partial\beta/\partial T$, is $1 \times 10^{-7}\,^{\circ}\mathrm{C}^{-2}$. It follows that a typical value of $\delta\beta$ is $1.4 \times 10^{-6}\,^{\circ}\mathrm{C}^{-1}$, or less than 1% of the calculated value. Note that the uncertainty in β is smaller than the estimated uncertainty in ε, which results from the specific data analysis process proposed in the current report.

References

[1] B.A. Boley, J.H. Weiner, Theory of Thermal Stresses, Wiley, USA, 1960.

[2] B.H. Dennis, G.S. Dulikravich, Y. Rabin, Optimization of organ freezing protocols with specified allowable thermal stress levels, in: International Mechanical Engineering Congress and Exposition 2000, Orlando, FL, November 5–10, HTD-Vol. 368/BED-Vol. 47, pp. 33–48.

[3] G.M. Fahy, D.R. MacFarlane, C.A. Angell, H.T. Meryman, Vitrification as an approach to cryopreservation, Cryobiology 21 (1984) 407–426.

[4] G.M. Fahy, Biological effects of vitrification and devitrification, in: D.E. Pegg, A.M. Karow Jr. (Eds.), Biophysics of Organ Cryopreservation, Plenum, New York, 1987, pp. 265–297.

[5] G.M. Fahy, J. Saur, R.J. Williams, Physical problems with the vitrification of large biological systems, Cryobiology 27 (1990) 492–510.

[6] A.A. Gage, J. Baust, Mechanisms of tissue injury in cryosurgery, Cryobiology 37 (3) (1998) 171–186.

[7] J.P. Holman, Experimental Methods for Engineers, seventh ed., McGraw-Hill, New York, 2001.

[8] J.P. Holman, Heat Transfer, ninth ed., McGraw-Hill, New York, 2002.

[9] B. Luyet, D. Rasmussen, Study by differential thermal analysis of the temperatures of instability of rapidly cooled solutions of glycerol, ethylene glycol, sucrose and glucose, Biomedica 10 (211) (1968) 167–191.

[10] P. Mazur, S. Leibo, E.H.Y. Chu, A two-factor hypothesis of freezing injury, Experimental Cell Research 71 (1972) 345–355.

[11] Y. Rabin, P.S. Steif, Analysis of thermal stresses around a cryosurgical probe, Cryobiology 33 (1996) 276–290.

[12] Y. Rabin, P.S. Steif, M.J. Taylor, T.B. Julian, N. Wolmark, An experimental study of the mechanical response of frozen biological tissues at cryogenic temperatures, Cryobiology 33 (1996) 472–482.

[13] Y. Rabin, P. Olson, M.J. Taylor, P.S. Steif, T.B. Julian, N. Wolmark, Gross damage accumulation in frozen rabbit liver due to mechanical stress at cryogenic temperatures, Cryobiology 34 (1997) 394–405.

[14] Y. Rabin, M.J. Taylor, N. Wolmark, Thermal expansion measurements of frozen biological tissues at cryogenic temperatures, ASME Journal of Biomechanical Engineering 120 (2) (1998) 259–266.

[15] Y. Rabin, P.S. Steif, Thermal stresses in a freezing sphere and its application to cryobiology, ASME Journal of Applied Mechanics 65 (2) (1998) 328–333.

[16] Y. Rabin, P.S. Steif, Thermal stress modeling of freezing biological tissues, in: Advances in Heat and Mass Transfer in Biotechnology, International Mechanical Engineering Congress and Exposition 1999, Nashville, TN, HTD-Vol. 363, BED-Vol. 44, pp. 183–188.

[17] Y. Rabin, P.S. Steif, P.S. Thermal, stress modeling in cryosurgery, International Journal of Solids and Structures 37 (2000) 2363–2375.

[18] Y. Rabin, A general model for the propagation of uncertainty in measurements into bioheat heat transfer simulations and its application to cryobiology, Cryobiology 46 (2) (2003) 109–120.